Soft Matter

Cite this: *Soft Matter*, 2012, **8**, 5020

www.rsc.org/softmatter

PAPER

Polymer surface texturing for direct inkjet patterning by atmospheric pressure plasma treatment†

Jae Beom Park,[a] Jae Yong Choi,[b] Suk Han Lee,[b] Yong Seol Song[c] and Geun Young Yeom*[a]

Received 5th December 2011, Accepted 20th February 2012
DOI: 10.1039/c2sm07305f

It would be beneficial if the substrate surface were treated to have hydrophobic properties, in order to keep the line pattern fine during the inkjet processing, while at the same time having improved adhesion properties on the substrate. In this study, a polyimide surface was textured using atmospheric pressure plasma treatment for fine line metal inkjet printing by micromasking the surface followed by etching the polyimide surface selectively. The water contact angle on the textured polyimide film was measured to be over 100 degrees, showing that the surface was hydrophobic. When the textured polyimide surface was printed on using an electro-hydro-dynamic inkjet for Ag line printing, not only fine line Ag printing, but also improved adhesion of Ag to the polyimide surface could be obtained while maintaining excellent resistivity. The improved adhesion properties in addition to the fine line patterning afforded by texturing the polyimide surface were caused by the increased surface contact area between the metal ink and the polyimide surface during the annealing of the Ag line.

1. Introduction

The manufacturing process of the microelectronic industry generally uses the photolithographic method, which consists of complicated process steps such as photomask fabrication, thin film deposition, spin-coating of a photoresist, ultraviolet (UV) light exposure, developing, and etching. These complicated, expensive, and time-consuming processes incur high manufacturing costs due to the expensive equipment required and the waste of expensive materials.[1–3] The application of a direct writing process such as ink-jet printing technology to microelectronic processing has various advantages, such as low cost, no waste of material, easier variation of the pattern shape, *etc.*, compared to the conventional lithographic method. Therefore, the ink-jet printing process is considered to be one of the next generation microelectronic processing technologies that can be applied to flat panel displays. In addition, the ink-jet printing process is potentially a low-temperature process that may enable manufacturing on flexible substrates. Also, it is compatible with continuous roll-to-roll processing and scales more favorably with increasing substrate area than the lithographic process.[4–8]

However, controlling the pattern size is a highly critical issue for the application of ink-jet printing to industrial manufacturing processes, especially for metal inkjet processing such as Ag, Cu, *etc.* Generally, the substrate heating method is used to obtain fine patterns during the inkjet process for the purpose of preventing the ink from spreading after printing on the substrate. But this method induces side effects such as the nozzle clogging effect, *etc.*[9–11] For example, H. Meier *et al.*[12] successfully printed 25 μm-width silver lines on a flat polyimide surface by controlling the droplet size. However, a heated substrate of 55 °C had to be used to obtain fine line patterns and, even though they did not mention it, a nozzle clogging effect will exist in addition to the adhesion problem. The control of the pattern size of the printed liquid depends on the surface-wetting properties; in other words, when water droplets are dropped onto a surface, the width and configuration of the droplet pattern are mainly determined by their surface-wetting properties. Typically, a hydrophilic surface has a small contact angle and is favorable to obtain good adhesion between the metal pattern and the surface of the substrate, but this hydrophilic surface is unfavorable in keeping the pattern width fine due to the spreading of the liquid. On the other hand, a substrate having hydrophobic surface characteristics has a large contact angle and tends to keep the pattern width of the inkjet extruding from the nozzle narrow. However, the printed inkjet pattern generally has poor adhesion to the substrate surface.[6,8,13] That is, both surface wetting properties, hydrophilic and hydrophobic, have unfavorable characteristics for metal fine line patterning using the inkjet printing process.

It would be beneficial if the substrate surface were treated so as to have hydrophobic properties, in order to keep the line pattern fine during the inkjet processing, while at the same time having

[a]*SKKU Advanced Institute of Nano Technology (SAINT), Sungkyunkwan University, Suwon, Kyunggi-do, South Korea 440-746. E-mail: gyyeom@skku.edu; Fax: +82-31-299-6565; Tel: +82-31-299-6560*
[b]*School of Information and Communication Engineering, Sungkyunkwan University, Suwon, Kyunggi-do, South Korea 440-746*
[c]*AMOGREENTECH 185-1 Tongjin-eup Gimpo, KyungGi-Do, South Korea 415-868*

† Electronic supplementary information (ESI) available. See DOI: 10.1039/c2sm07305f

improved adhesion properties on the substrate. In this study, the polyimide surface was treated by atmospheric plasmas to form a microscopic texture such as a lotus surface. The formation of a micro- or nanostructure to achieve a superhydrophobic surface has been investigated by many other researchers using various processes such as polymer imprinting, self-assembly, *etc.*[14–18] However, these processes are complicated, expensive, or difficult to scale to large area processing. By using atmospheric pressure plasmas, the microscopic structures could be more easily formed on large area substrates through in-line or roll-to-roll processing, both reproducibly and efficiently.

In addition, when microtexturing similar to a lotus surface was formed on the polyimide surface by atmospheric pressure plasma treatment composed of micromasking processing and selective etch processing, not only a hydrophobic surface which maintains a fine line pattern during the inkjet processing, but also improved adhesion properties could be obtained. The improved adhesion properties were caused by the increased contact surface area between the inkjet metal line pattern and the polyimide surface, due to the microstructure of the polyimide surface.

2. Experimental

Atmospheric discharge system

The atmospheric discharge system used in this experiment is shown in Fig. 1. The system was composed of four electrodes. The upper electrode was itself composed of 3 electrodes (two power electrodes and one ground electrode) to form a remote plasma configuration. The lower electrode which is located below the substrate was grounded for the remote plasma configuration or connected to a separate power supply for the biased configuration. All of the electrodes were covered with a 2 mm thick Al_2O_3 plate. The discharge gap of the upper electrodes was 5 mm and the discharge gap between the upper electrodes and lower electrode was 15 mm. The upper electrode was connected to an AC power supply with a frequency of 30 kHz and the input power was fixed at 360 W (an electrode voltage of about 7 kV). The lower electrode was grounded or connected to a quasi-pulse power supply with a frequency of 60 kHz. The input power to the lower electrode for the biased condition was varied from 200 W to 1000 W in this study. This double atmospheric discharge system with the configuration of a bottom discharge in addition to a top remote-type plasma showed a higher process efficiency compared with other conventional dielectric barrier discharge systems, due to the larger discharge area and higher gas dissociation efficiency near the substrate.

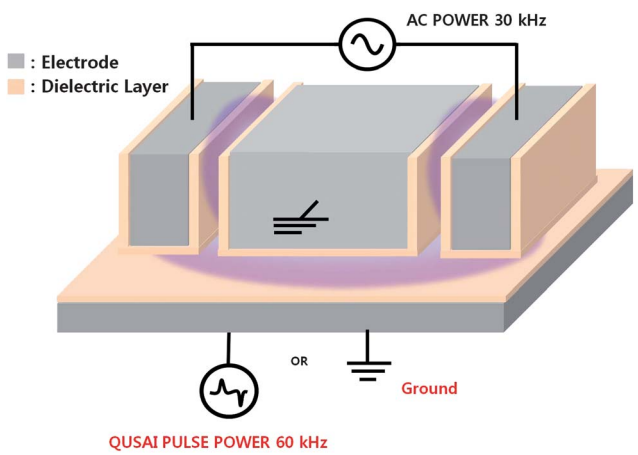

Fig. 1 Schematic diagram of a double dielectric barrier discharge-type atmospheric pressure plasma system used in the experiment.

Polymer substrate

A 50 μm thick polyimide film (SKC KOLON, Gyeonnggi-do, Korea), which has a PDMA-ODA structure, was used as the substrate in this study.

Gas mixture for atmospheric discharge

For the deposition of a thin silicon oxide mask layer on the polyimide film, a hexamethyldisilazane (HMDS)/He/O_2 gas mixture for the deposition of the mask layer and a He/O_2 gas mixture for its agglomeration and oxidation were used. For the selective etching of the polyimide surface, a He/O_2/Ar gas mixture was used and, for the removal of the mask layer, an N_2/NF_3 gas mixture was used.

Direct inkjet process

For the dot and line patterning of Ag ink, an electrostatic field induced inkjet head called the electro-hydro-dynamic (EHD) printing system, based on EHD discharging of tiny droplets, in which drop and jet are formed by an induced electric field was used and the details of the printing technology can be found in ref. 19. The ink used in this study (NPS-J, HARIMA Chemical, Inc.) was about 57 wt% suspension of silver nanoparticles, whose sizes ranged between 8 and 15 nm, and dispersed in tetradecane. The viscosity and surface tension of the ink were 7–11 mPa s and 26.56 mN m^{-1} at room temperature, respectively.

Analyzer and measurement systems

The contact angles of deionized water on the treated (that is, textured) and untreated polyimide film surfaces were measured using a contact angle analyzer (SEO, Phoenix 450). The surface images of the treated and untreated polyimide surface morphologies were investigated by using a field emission scanning electron microscope (FE-SEM: HITACHI, s-4700). The chemical information on the treated and untreated polyimide film surface was obtained using X-ray photoelectron spectroscopy (XPS: Thermo VG SIGMA PROBE). The adhesion test was progressed by using the tape method. The 3M scotch tape was used for the adhesion test, and the Ag pattern shapes before and after the taping were compared.

3. Results and discussion

SEM image of polymer surface

The texturing process of the polyimide substrate surface was composed of four steps. Fig. 2 shows the process flow for the polyimide microstructure texturing using atmospheric pressure plasmas and the SEM images of the polyimide film surface after each step: HMDS deposition (step 1), micromasking process (step 2), selective etching of polyimide (step 3), and mask removal

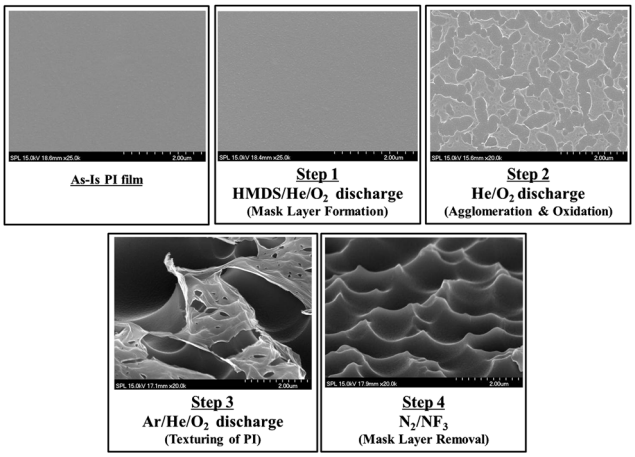

Fig. 2 The process flow for polyimide microstructure texturing using atmospheric pressure plasmas, and the SEM images of the polyimide film surface after the each step: HMDS deposition (step 1), micromasking process (step 2), selective etching of polyimide (step 3), and mask removal (step 4).

(step 4). During the 1st process step, a thin HMDS layer was deposited for 5 seconds on the polyimide film using the atmospheric discharge system. A gas mixture of HMDS (75 sccm)/He (10 slm)/O_2 (10 slm) and top/bottom power of 360 W/200 W were used for the atmospheric discharge during the 1st step. In the 2nd process step, the agglomeration and oxidation of HMDS were conducted to form an HMDSO micromask for the subsequent selective polyimide etching process by exposing an atmospheric pressure plasma of He (10 slm)/O_2 (15 slm) for 1 minute. During the 2nd step, the bottom power was varied from 400 to 1000 W, while keeping the top electrode power at 360 W. In the 3rd step, microstructural texturing by the selective etching of the surface using the HMDSO mask layer was conducted using an atmospheric pressure plasma composed of a gas mixture of He (10 slm)/O_2 (15 slm)/Ar (10 slm) for 1 minute. During the 3rd step, the top/bottom electrode powers were maintained at 360 W/1 kW. After the selective etching of the polyimide surface, the HMDSO mask layer was removed by an atmospheric discharge composed of N_2 (40 slm)/NF_3 (3 slm) by applying 1 kW to the top electrode. The polyimide film was processed at a speed of 0.25 m min^{-1}.

Atomic percentage of textured polyimide surface

The surface composition of the polyimide surface after each step of the atmospheric pressure plasma treatment shown in Fig. 2 was measured by XPS and the result is shown in Table 1. In step 2, the bias power to the bottom electrode was maintained at 1 kW. As shown in the table, before the treatment, the surface was composed of carbon (71.64%), oxygen (20.24%), and nitrogen (8.12%), however, after the HMDS coating, silicon (0.46%) was formed on the surface and its percentage appeared to be increased to 6.44% by the oxidation and agglomeration of HMDS by the He/O_2 plasma treatment during the 2nd step. In fact, no silicon source was used in this step, however, by the oxidation and agglomeration of HMDS by the He/O_2 plasma treatment during the 2nd step, the silicon percentage appeared to be increased relatively because of the decrease of carbon on the surface. During the selective etching of the polyimide surface, the surface composition remained similar to that of the 2nd step, indicating that there was no change in the properties of the HMDSO mask during the selective etching. After the plasma treatment using N_2/NF_3 in the 4th step, the HMDSO mask layer was completely removed so the silicon related peak was not observed on the etched polyimide surface. However, after the N_2/NF_3 plasma treatment, about 64.49% of F, which is caused by the formation of C–F bonding on the polyimide surface, was observed on the polyimide surface.

Table 1 Atomic percentages measured by XPS on the plasma treated polymer surface as a function of each process step

Process step	Si (at%)	Oxy (at%)	C (at%)	N (at%)	F (at%)
As-Is	X	20.24	71.64	8.12	X
Step 1	0.46	28.05	56.26	15.23	X
Step 2	6.44	42.48	36.76	14.32	X
Step 3	6.64	43.54	34.81	15.01	X
Step 4	X	5.04	27.31	3.16	64.49

Morphology of HMDSO mask layer on the polyimide surface

Fig. 3 shows the morphology of the HMDSO mask layer coated on the polyimide surface as a function of the bias power to the substrate during the 2nd step of agglomeration and oxidation after the deposition of the thin HMDS layer. After its deposition on the substrate, the thin HMDS layer was agglomerated and oxidized for 1 minute by applying a bias power to the substrate in the range from 400 W to 1000 W, while operating a remote-type He (10 slm)/O_2 (15 slm) atmospheric pressure plasma with an AC power of 360 W. As shown in Fig. 2, when a bias power of 400 W

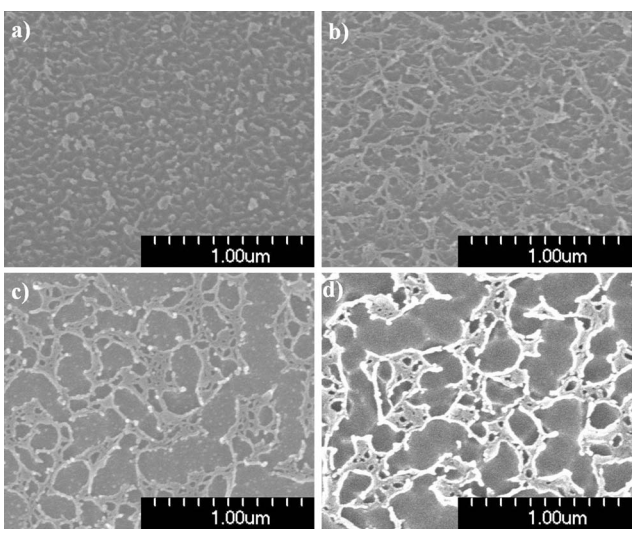

Fig. 3 Morphology of the HMDSO mask layer coated on the polyimide surface as a function of the bias power to the substrate during the 2nd step of agglomeration and oxidation after the deposition of a thin HMDS layer. After the deposition of the thin HMDS layer on the substrate, the layer was agglomerated and oxidized for one minute by applying bias powers to the substrate ranging from 400 W to 1000 W, while operating a remote-type He (10 slm)/O_2 (15 slm) atmospheric pressure plasma. (a) 400 W, (b) 600 W, (c) 800 W, and (d) 1000 W.

was applied, only part of the surface area of the deposited thin HMDS layer was agglomerated, showing 100–200 nm diameter particle-type HMDSO on the polyimide surface. By increasing the bias power to 600 W, a fiber (or ribbon)-type network of HMDSO with a size of a few hundred nanometres could be observed due to its agglomeration. When increasing the bias power to 1000 W, the HMDSO was further agglomerated into a thin fiber (or ribbon)-type network and the exposed polyimide surface area was increased. It is believed that the agglomeration of HMDSO is related to the increased stress in the film during the oxidation and C–H removal of the deposited HMDS thin film and the increased mobility of the surface atoms caused by the increased ion bombardment (or heating) at the increased bias power.[20,21]

Oxidation of HMDSO mask layer

Fig. 4 shows the chemical bonding state of the Si 2p in the HMDSO formed on the polyimide surface during the 2nd step measured as a function of the bias power (400–1000 W), while operating a remote-type He (10 slm)/O_2 (15 slm) atmospheric pressure plasma with an AC power of 360 W. As shown in the figure, with increasing bias power, the binding energy and intensity of the Si 2p peak were also increased. The Si 2p peak position was 102.21 eV for 400 W and 102.91 eV for 600 W, which are lower than the value of 103.3 eV for Si–O_2 bonding and higher than the value of 102.1 eV for $(CH_3)_2$–Si–O_2 bonding.[22,23] Therefore, the HMDS layer formed on the polyimide surface was not sufficiently oxidized by the He/O_2 plasma during the 2nd step when the bias power was less than or equal to 600 W. In addition, due to the low oxidation and agglomeration of HMDS, the peak intensity of Si 2p was low. However, the Si 2p peak was increased to 103.26 eV at a bias power of 800 W and 104.07 eV at 1000 W, which is close to the silicon bonding to Si–O_2 bonding at 103.3 eV and Si–(O or $OH)_4$ bonding at 104.3 eV, in addition to the increase of the Si 2p peak intensity due to the further agglomeration on the polyimide surface.

Contact angle of textured polyimide surface

The degree of surface texturing after the surface treatment by the atmospheric pressure plasmas was observed by FE-SEM and the result is shown in Fig. 5. During the 2nd step, bias powers of 600 W and 1000 W were applied for Fig. 5(a) and (b), respectively. In the case of Fig. 5(c) the 1st step HMDS coating time was increased to 9 seconds instead of 5 seconds (for Fig. 5(a) and (b)), while keeping the bias power at 1000 W during the 2nd step. As shown in Fig. 5(a), when the bias power during the 2nd step was 600 W, the degree of surface texturing of the polyimide was low, showing triangular features with a low aspect ratio and obtuse angle. However, when the bias power was increased to 1000 W, as shown in Fig. 5(b), a rougher polyimide surface was observed, showing triangular features with a high aspect ratio and acute triangles. The low surface texturing obtained in Fig. 5(a) is believed to be related to the less selective mask formed by the incomplete oxidation of HMDS in Fig. 3(b), while the higher surface texturing for Fig. 5(b) is related to the formation of a more selective mask during the 2nd step through the greater oxidation of HMDS, as shown in Fig.3(d) and the first picture of Fig. 5(b). However, as shown in Fig. 5(c), when the 1st step time was increased to 9 seconds from 5 seconds, while keeping the bias power in the 2nd step at 1000 W, due to the too thick HMDS thin film formed on the polyimide surface during the 1st step, most of the polyimide surface was covered with HMDSO even after the oxidation and agglomeration step and, therefore, only part of the polyimide surface was etched.

The contact angle before and after the plasma treatment was measured using a contact angle analyzer and the results are also shown in Fig. 5. Before the plasma treatment, the contact angle on the polyimide surface was about 33.4°. However, after the treatment using a bias power of 600 W, the contact angle increased to 83.5°, as shown in Fig. 5(a), and, when the bias power was increased to 1 kW (Fig. 5b), the contact angle was further increased to 105.7°. The increase of the 1st step HMDS formation time from 5 seconds to 9 seconds, however, decreased the contact angle to 67.8°, although it is still higher than that of

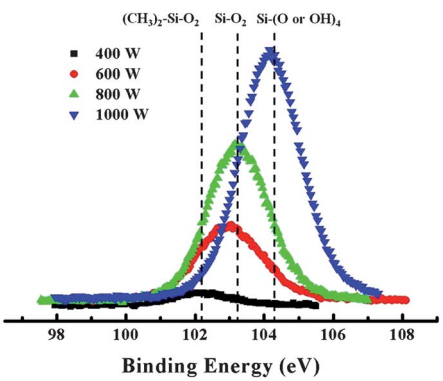

Fig. 4 XPS chemical bonding state of the Si 2p peak in the HMDSO formed on the polyimide surface during the 2nd step measured as a function of the bias power in Fig. 3. The process condition is same as that in Fig. 3.

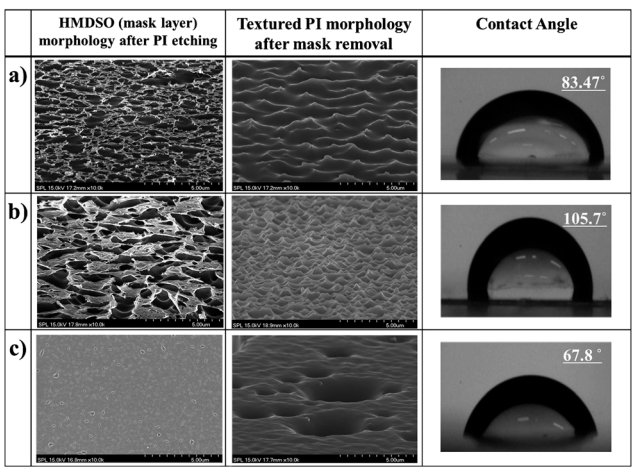

Fig. 5 The degree of surface texturing observed by FE-SEM after the surface treatment using the atmospheric pressure plasmas. The first pictures are after the selective polyimide etching (step 3) and the second pictures are after the HMDSO mask removal (step 4). During the 2nd step, a bias power of 600 W was applied for (a), while a bias power of 1000 W was applied for (b). In the case of (c) the 1st step HMDS coating time was increased to 9 seconds instead of 5 seconds, while keeping the bias power of the 2nd step at 1000 W. The contact angles after the texturing are also shown.

the untreated polyimide surface. (When the contact angle was measured with the tetradecane solution which is the inkjet solution instead of DI water, complete spreading having a near 0° contact angle was observed for the untreated polyimide surface. When the polyimide was treated with the NF_3/N_2 atmospheric remote plasma treatment (4th process step), the contact angle was increased to 36.7° and, in the case of the plasma textured polyimide, the contact angle was further increased to 77.6°(Fig. A-3†). Therefore, by using the tetradecane solution, even though the contact angle similar to that of DI water could not be obtained, the highest contact angle could be obtained on the plasma textured polyimide.)

Contact angle hysteresis of plasma texture polyimide surface

Using the polyimide surface textured using the condition in Fig. 5(b) (having a contact angle of 105.7° with 1000 W of bias power in the 2nd process step, 5 s of the 1st process time), the contact angle hysteresis was measured and the results are shown in Fig. 6 and Table 2 for slope angles from 10° to 45°. As shown in Fig. 6, as the polyimide surface was tilted, the water droplet remained on the polyimide surface, while showing differences in the advancing contact angle and receding contact angle, and, at 45°, the contact angle hysteresis was increased to 36.6°. In general, for a substrate having hydrophobic characteristics, the contact angle hysteresis is generally small and the droplet easily runs away at a small angle of tilting, while it also has a high contact angle larger than >100° producing an effect like that of a droplet on a lotus leaf. Therefore, the adhesion between the substrate and the droplet is very poor. However, in the case of the polyimide surface treated by the atmospheric pressure plasma, not only hydrophobic characteristics, but also high contact angle hysteresis which may indicate hydrophilic characteristics could be observed.

Two hydrophobic surface models, *viz.* the Wenzel model (eqn (1)) and the Cassie model (eqn (2)), have been suggested for textured surfaces,[24,25]

$$\cos\theta^{W} = r\cos\theta \quad (1)$$

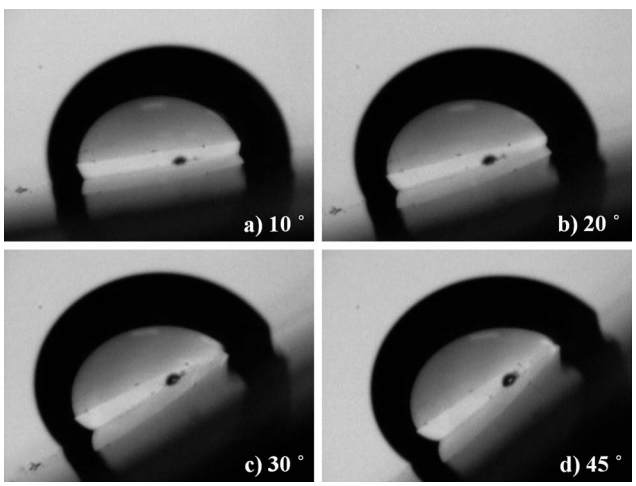

Fig. 6 Images of the contact angle showing the hysteresis of the contact angle as a function of the polymer substrate tilting angle of (a) 10°, (b) 20°, (c) 30°, and (d) 45°.

$$\cos\theta^{C} = -1 + \Phi_S(1 + \cos\theta) \quad (2)$$

where θ^W and θ^C are the contact angles of the hydrophobic surface when the surface follows the Wenzel and Cassie models after the surface texturing, respectively, θ is Young's contact angle (determined on a flat surface, and measured to be 61° after the NF_3/N_2 plasma treatment of step 4 in Fig. 2 on a flat polyimide surface), r is defined as the ratio of the actual to the apparent surface area of the substrate (r is a number larger than unity), and Φ_S is defined as the fraction of solid in contact with the liquid. (In this experiment, r was approximately calculated to be 1.55 and Φ_S to be 0.45 by assuming that the triangular features in Fig. 8(a) are partially truncated pyramid shapes of 1 μm length × 0.6 μm height having 40% of flat area on the top of the pyramids.) The schematic diagrams of the models are shown in Fig. 7. For the polyimide surface treated by the condition in Fig. 5b, when the surface textured feature is assumed to be a pyramid shape, after the surface texturing, the contact angle is supposed to change to 41° for the Wenzel model and to 109° for the Cassie model. Therefore, our textured polyimide surface appears to follow the Cassie model. However, for the Cassie model, the substrate surface tends to show contact angle hysteresis, while the substrate surface shows a hydrophobic surface.[26] The reason for the high contact angle hysteresis while following the Cassie model could be partially related to the change of the polyimide surface properties after the N_2/NF_3 plasma treatment, as shown in Table 2, and partially to the microroughness formed on the top of the triangular features, in addition to the large acute triangular features (shown in Fig. 8(a)), which hold the droplet on the substrate (which may indicate a Cassie–Wenzel combined model in Fig. 8(b).

In fact, the increase of the contact angle hysteresis by the additional microfeatures on the macrofeatures has been previously reported by other researchers.[27] In our experiment, the formation of the microroughness on top of the triangular features in Fig. 8(a) is believed to be related to the porous nature of the HMDSO mask layer formed on the polyimide surface.

Pattern width of Ag ink on plasma textured polyimide

On the polyimide surface treated by the condition in Fig. 5(b), Ag ink was dropped and its patterning property was investigated. Fig. 9 shows the optical microscopic images of the Ag pattern formed on the polyimide surface before and after the treatment with the condition in Fig. 5(b). The nozzle size of the inkjet head was 38 μm. After the formation of the dot pattern, the patterned polyimide was sintered for 15 minutes at 230°. The solvent used for the Ag ink was tetradecane, which has a surface tension of 26.56 mN m^{-1} at 20 °C, while the surface tension of H_2O is 71.97 mN m^{-1}. Therefore, the Ag ink tends to show a lower contact angle compared to the water droplet, due to the low surface tension, and, as shown in the figure, the droplet size on the untreated polyimide surface was 120–140 μm, which is about 4–5 times larger than the nozzle size. However, in the case of the polyimide surface textured by the atmospheric pressure plasma with the condition in Fig. 5(b), a decrease of the Ag pattern size to about 60 μm was observed. Therefore, even though an increase of the Ag pattern size compared to the nozzle size was obtained, due to the extremely low surface tension of the Ag ink,

Table 2 DI water contact angle (advancing and receding) and contact angle hysteresis of a plasma treated polyimide surface having a nano-microstructure

Tilted substrate angle/degree	Advancing CA/degree	Receding CA/degree	CA hysteresis/ degree
10	106.2	96.25	**9.95**
20	107	88.65	**18.35**
30	108.4	83.18	**25.22**
45	114.88	78.24	**36.64**

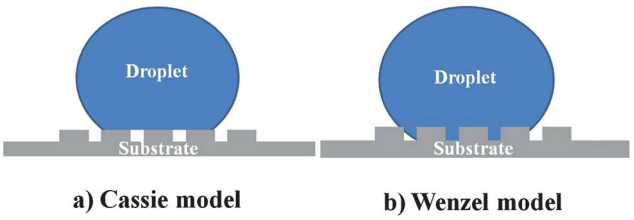

Fig. 7 Schematic diagrams of (a) the Cassie model and (b) the Wenzel model for contact angle on a roughened surface.

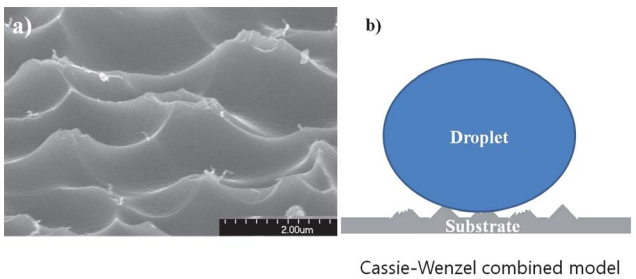

Fig. 8 (a) SEM images of a textured polyimide surface showing microroughness on the top of triangular features. (b) A Cassie–Wenzel combined model for a textured surface having higher contact angle and larger contact angle hysteresis after texturing.

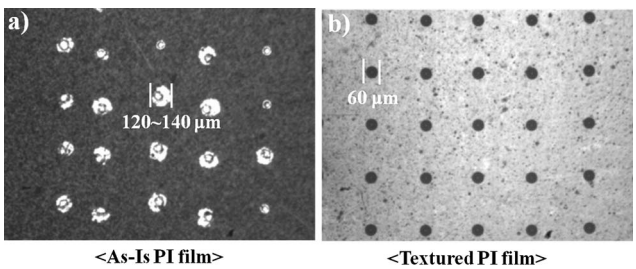

Fig. 9 Optical microscope images of Ag dot pattern formed by an inkjet printing system on the polyimide surface before (a) and after (b) texturing using atmospheric pressure plasmas.

a significant decrease of the Ag pattern width was obtained by the texturing of the polyimide surface using the atmospheric pressure plasma treatment.

Adhesion properties of the Ag ink pattern on plasma texture polyimide

The adhesion properties of the Ag ink pattern on the polyimide surface before and after the texturing by the atmospheric pressure plasma shown in Fig. 9 are shown in Fig. 10(a). On the polyimide surface treated and untreated by the plasma, Ag dot and line patterns were formed, respectively, and the degree of adhesion was tested by tape testing using 3M tape after sintering with the condition in Fig. 9. As shown in the figure, the Ag pattern formed on the untreated polyimide surface was easily peeled off, as shown in the bottom sample picture of Fig. 10(a) and, also, when the interface between the polyimide and Ag pattern was observed by SEM, as shown in Fig. 10(b), the interface was split, indicating poor adhesion between the polyimide and the Ag pattern. In fact, it is known that the adhesion force between a polymer and noble metal is generally low.[28–31] However, the surface texturing by the atmospheric pressure plasma improved the adhesion, as confirmed by the absence of an Ag pattern after the tape testing in the top sample picture of Fig. 10(a). Therefore, due to the surface texturing by the plasma treatment, not only a decrease in the width of the Ag ink pattern, but also an increase of its adhesion to the polyimide surface could be obtained.

The decrease in the width of the Ag pattern after the surface texturing by the atmospheric pressure plasma is believed to be related to the increased contact angle observed in Fig. 5(b), even though the Ag ink used in the experiment may show a lower contact angle compared to H_2O, due to the lower surface tension. However, the improved adhesion of the Ag pattern to the substrate after the surface texturing appears to be more related to the increased contact area between the polymer and Ag pattern, in the manner of the contact of the Wenzel model, by filling the Ag ink into the valleys and hills of the triangular features on the

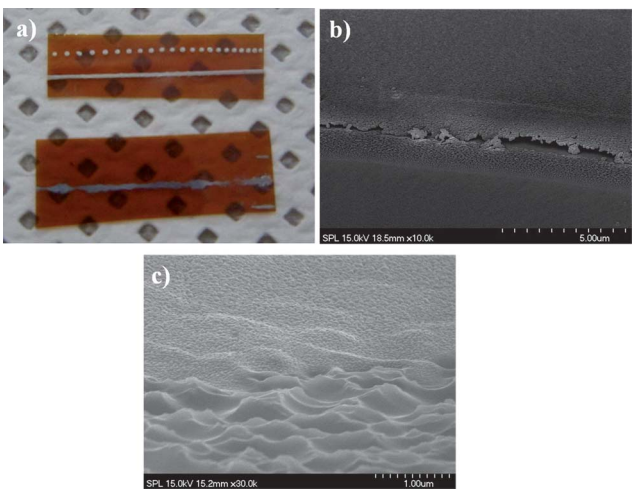

Fig. 10 (a) Photograph of polyimide films patterned with Ag ink followed by peeling off the pattern using 3M scotch tape to compare the adhesion force before and after the texturing using atmospheric pressure plasma treatment: (top image) the Ag ink pattern on the plasma textured polyimide and (bottom image) the Ag ink pattern on the untreated polyimide after peeling off using 3M scotch tape. (b) SEM image showing a crack between the Ag metal pattern and the polyimide surface for the non-plasma treated polyimide, indicating poor adhesion. (c) SEM image showing the boundary between the Ag pattern and polyimide surface for the textured polyimide after the Ag ink sintering. The Ag ink was filling into the valleys and hills of the triangular features on the polyimide textured surface during the sintering process.

polyimide textured surface during the sintering process, as shown in Fig. 10(c), in addition to the microfeatures observed in Fig. 8 which cause an increase in the contact angle hysteresis for the water droplet.

4. Conclusions

In this study, a polyimide surface was textured using multiple-step atmospheric pressure plasma treatment composed of HMDS deposition, oxidation and agglomeration of HMDS for micromask formation, selective polyimide etching, and mask etching, and the characteristics of the polyimide surface for Ag inkjet printing, such as its hydrophobicity and adhesion characteristics, were investigated. The degree of texturing of the polyimide surface was dependent on the process conditions during the atmospheric pressure plasma treatment. Especially, when the bias power to the substrate was varied during the mask oxidation and agglomeration of HMDS, surface texturing features with different aspect ratios, different shapes, and different feature densities could be obtained, due to the differences in the agglomeration of the HMDS used for the formation of the micromask. Under the optimized conditions, due to the surface texturing, the contact angle was increased from 33.4° to 105.7° and this increase was related to the Cassie model, similar to the contact of a water droplet on a lotus leaf. However, when the contact angle hysteresis was measured, a high contact angle hysteresis of 36.6° was observed at a tilting angle of 45°, which is more related to the hydrophilic surface properties. The high contact angle hysteresis is believed to be related to the change of the polymer surface properties and the formation of micro-roughness on the top of the textured features, which cause the properties to follow a Cassie–Wenzel combined model. Due to the improved adhesion properties, in addition to the increased hydrophobic surface properties after the texturing of the polyimide surface caused by the atmospheric pressure plasma treatment, when Ag metal ink was patterned on the polyimide surface by an Ag inkjet, a significant improvement in the fine line patterning in addition to the increased adhesion of the Ag metal pattern compared to those on the untreated polyimide surface was observed, which is ideal for the metal inkjet patterning on the flexible substrate. Especially, for the metal inkjet patterning, the improved adhesion properties were caused by the increased surface contact area between the metal ink and the polyimide surface during the sintering of the Ag ink by the filling of the valleys and hills of the textured features on the polyimide surface. It is believed that the surface texturing method used in this experiment can be easily applied to flexible polymer substrates, such as polyimide, *etc.*, which have problems in terms of their adhesion and fine line patterning during noble metal line formation using an ink jet through in-line processing or roll-to-roll processing.

Acknowledgements

This work was carried out through the Direct Nano Patterning Project supported by the Ministry of Knowledge Economy (MKE) under the National Strategic Technology Program, and by the World Class University program (grant no. R32-2008-000-10124-0) of the National Research Foundation of Korea (NRF) funded by the Ministry of Education, Science, and Technology.

References

1 D. Kim, S. Jeong, S. Lee, B. K. Park and J. Moon, *Thin Solid Films*, 2007, **515**, 7692.
2 B. K. Park, D. Kim, S. Jeong, J. Moon and J. S. Kim, *Thin Solid Films*, 2007, **515**, 7706.
3 S. M. Bidoki, D. M. Lewis, M. Clark, A. Vakorov, P. A. Millner and D. McGorman, *J. Micromech. Microeng.*, 2007, **7**, 967.
4 Y. Wang, J. Bokor and A. Lee, *Emerging Lithographic Technologies VIII: Proc. SPIE*, 2004, **5374**, 628.
5 Y. Liu, K. Varahramyan and T. Cui, *Macromol. Rapid Commun.*, 2005, **26**, 1955.
6 B. J. de Gans, P. C. Duineveld and U. S. Schubert, *Adv. Mater.*, 2004, **16**, 203.
7 B. J. de Gans and U. S. Schubert, *Macromol. Rapid Commun.*, 2003, **24**, 659.
8 C. W. Sele, T. von Werne, R. H. Friend and H. Sirringhaus, *Adv. Mater.*, 2005, **17**, 997.
9 J. Perelaer, B. J. de Gans and U. S. Schubert, *Adv. Mater.*, 2006, **18**, 2101.
10 Z. Liu, Y. Su and K. Varahramyan, *Thin Solid Films*, 2005, **478**, 275.
11 S. B. Fuller, E. J. Wilhelm and J. M. Jacobson, *J. Microelectromech. Syst.*, 2002, **11**, 54.
12 H. Meier, U. Löffelmann, D. Mager, P. J. Smith and J. G. Korvink, *Phys. Status Solidi A*, 2009, **206**, 16267.
13 K. Murata, J. Matsumoto, A. Tezuka, Y. Matsuba and H. Yokoyama, *Microsyst. Technol.*, 2005, **12**, 2.
14 Y. Lee, S. H. Park, K. B. Kim and J. K. Lee, *Adv. Mater.*, 2007, **19**, 2330.
15 H. Y. Erbıl, A. L. Demirel, Y. Avcı and O. Mert, *Science*, 2003, **299**, 1377.
16 X. Feng and L. Jiang, *Adv. Mater.*, 2006, **18**, 3063.
17 L. Zhai, F. C. Cebeci, R. E. Cohen and M. F. Rubner, *Nano Lett.*, 2004, **4**, 1349.
18 G. Jin, H. J. Jeon and G. H. Kim, *Soft Matter*, 2011, **7**, 4723.
19 J. C. Choi, Y. J. Kim, S. H. Lee, S. U. Son, H. S. Ko, V. D. Nguyen and D. Y. Byun, *Appl. Phys. Lett.*, 2008, **93**, 193508.
20 H. Cheng, A. Wu, J. Xiao, N. Shi and L. Wen, *J. Mater. Sci. Technol.*, 2009, **25**, 489.
21 C. Doughty, D. C. Knick, J. B. Bailey and J. E. Spencer, *J. Vac. Sci. Technol., A*, 1999, **171**, 2612.
22 M. R. Alexander, R. D. Short, F. R. Jones, W. Michaeli and C. J. Blomfield, *Appl. Surf. Sci.*, 1999, **137**, 179.
23 J. Viard, E. Beche, D. Perarnau, R. Berjoan and J. Durand, *J. Eur. Ceram. Soc.*, 1997, **17**, 2025.
24 R. N. Wenzel, *Ind. Eng. Chem.*, 1936, **28**, 988.
25 A. B. D. Cassie and S. Baxter, *Trans. Faraday Soc.*, 1944, **40**, 546.
26 A. Lafuma and D. Quéré, *Nat. Mater.*, 2003, **2**, 457.
27 D. Zahner, J. Abagat, F. Svec, J. M. J. Fréchet and P. A. Levkin, *Adv. Mater.*, 2011, **23**, 673.
28 S. H. Kim, S. W. Na, N. E. Lee, Y. W. Nam and Y. H. Kim, *Surf. Coat. Technol.*, 2005, **200**, 2072.
29 S. H. Kim, S. H. Cho, N. E. Lee, H. M. Kim, Y. W. Nam and Y. H. Kim, *Surf. Coat. Technol.*, 2005, **193**, 101.
30 A. K. S. Ang, E. T. Kang, K. G. Neoh, K. L. Tan, C. Q. Cui and B. T. Lim, *Polymer*, 2000, **41**, 489.
31 A. Weber, A. Dietz, R. Pockelmann and C. P. Klages, *J. Electrochem. Soc.*, 1997, **3**, 1131.